Efficient and stable operation of bearingless motors using a Hall sensors arrangement method for angle detection with less magnetic interference

Masahito MIYOSHI*, Yuichiro NAKAMURA*, Katsuya YAMAJI*
*Advanced Technology R&D Center, Mitsubishi Electric Corporation, Japan
8-1-1, Tsukaguchi-Honmachi, Amagasaki City, Hyogo 661-8661, Japan
E-mail: Miyoshi.Masahito@ay.MitsubishiElectric.co.jp

Abstract
This paper describes a Hall sensors arrangement method of bearingless motors to reduce the effect of magnetic flux from windings on rotor angle detection. The arrangement method needs no additional magnets or no sophisticated controls, and focuses on the combination of poles/slots and the placement of Hall sensors. An angle error caused by windings contains components of offset from DC current and harmonics from PWM ripple current. It is known that the detected angle error shifts the direction of suspension force generated in the XY plane and sometimes have a negative impact on radial suspension performance. This paper also shows that the interference from current can destabilize rotation control and cause divergence of speed oscillation. Results of FEM and simulation using block diagrams show the proposed method effectively reduces the effect of current on the angle error, and both rotation control and suspension control can be improved.

Keywords : Bearingless, Angle detection, Hall sensor, Magnetic interference, PWM harmonics

1. Introduction

Bearingless motors integrate magnetic bearings and the motor, levitating and rotating in a non-contact manner. Generating suspension force and torque as intended requires detecting the accurate rotor angle and determining phase of currents of suspension windings and motor windings. Hall-effect sensors are often used for rotor angle detection of the bearingless motors. The magnetic flux of the rotor magnet enables contactless position detection. However, currents in the stator windings also generate magnetic flux in the surrounding area, which may have a harmful effect on accuracy of angle detection (Peralta et al., 2020, Rao et al., 2015). The distortion in detected angle can be seen even with open-loop control that does not use detected angle in control, but closed-loop speed control can sometimes deteriorate speed oscillation (Weinreb, 2020). Eddy current also complicates transients and the correlation between flux distribution and coil currents (Rudolph et al., 2013, 2014).

Adding hall sensors or considering dynamic model can be strategies of compensation for current disturbance (Horikawa et al., 2013). It is also necessary to note that harmonic currents due to PWM switching control pulsate the Hall sensor signal. The pulsating noise is superimposed on the feedback value for position control, which causes an oscillation problem in magnetic suspension system. Holding the Hall sensor output can greatly decrease the pulsating noise (Egawa et al., 2021). However, the signal-hold method could deteriorate responsiveness, or remain the average position error if the sampling timing is incorrect.

The authors have presented a solution to the problem of the magnetic interference from both motor windings and suspension windings (Miyoshi et al., 2024). 10-poles 12-slots bearingless motors can enable the six Hall sensors to be arranged so that the influence of adjacent windings weaken each other. It can be applied without any increase in cost or motor volume.

This paper shows the improvement of stability in the proposed Hall Sensors arrangement in FEM and simulation using block diagrams. A condition under which the rotational control becomes unstable and speed oscillations occur is mathematically derived in this paper, and control performance is improved in the proposed arrangement.

2. Hall sensors arrangement method for angle detection with less magnetic interference

Figure 1 shows well-known angular error factors and a compensation method. Figure 1(a) shows the configuration of a two-axis control type bearingless motor with 10 poles and 12 slots and suspension windings that generate a magnetic field of 8 poles. The angle is detected by the magnetic flux of the rotor magnet using six Hall sensors in slots. For miniaturization, six Hall-sensors are installed in slots near windings. In fig. 1(a), stray flux from the U-phase suspension windings strengthens one of the magnet fluxes and weakens the magnet flux at the opposite side. The interference causes an error of angle detection. Figure 1(b) shows the rotor deviation in the radial and tilt directions. The rotor deviation disturbs the magnetic flux distribution in a similar way.

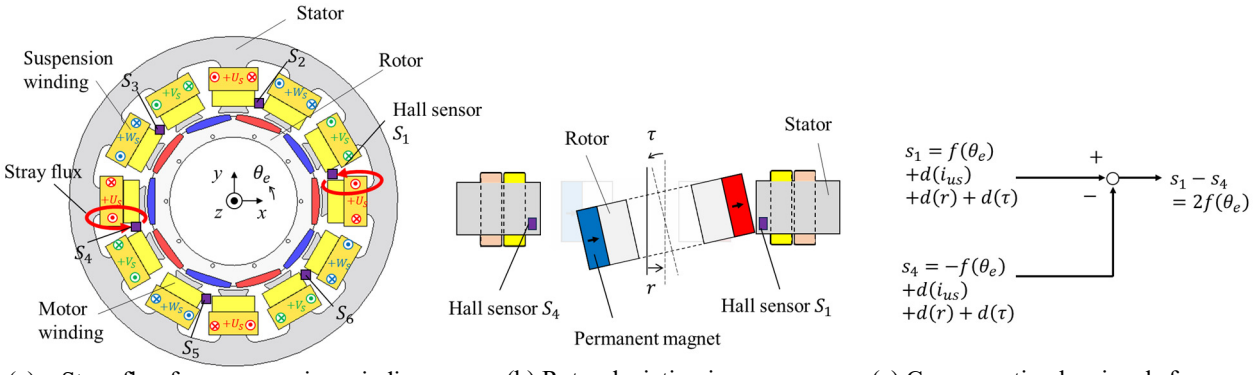

(a) Stray flux from suspension windings (b) Rotor deviation in radial and tilt directions (c) Compensation by signals from two opposing sensors

Fig. 1 Factors of error in angle detection and a compensation method.

It is known that these effects can be compensated for by utilizing two sensors that are 180 degrees opposite each other (Peralta et al., 2020). If the number of pole pairs is odd, then by taking the difference between the signals of the two sensors $(s_1 - s_4, s_3 - s_6, s_5 - s_2)$, the desired signal term f due to the angle θ_e of the rotor PM is amplified and the disturbance terms d due to the suspension current i_s and rotor deviation r, τ are cancelled in fig. 1(c).

On the other hand, the stray flux caused by the motor windings cannot be compensated for by difference operations. This is because the number of poles in the motor winding is the same as the number of poles in the magnetic flux of the permanent magnet. It is impossible to amplify the PM flux and cancel the motor winding flux simultaneously in a sum or difference calculation.

Therefore, this paper focus on the pole-slot selection. If the ratio of the number of poles to the number of slots is 2:3 or 4:3, motor windings in the same phase do not continue. However, if 10 poles and 12 slots are selected as the ratio between them, there are slots with coils in the same phase on both sides.

Figure 2(a) shows a comparative configuration. The location of the Hall sensors is incorrectly selected, the magnetic

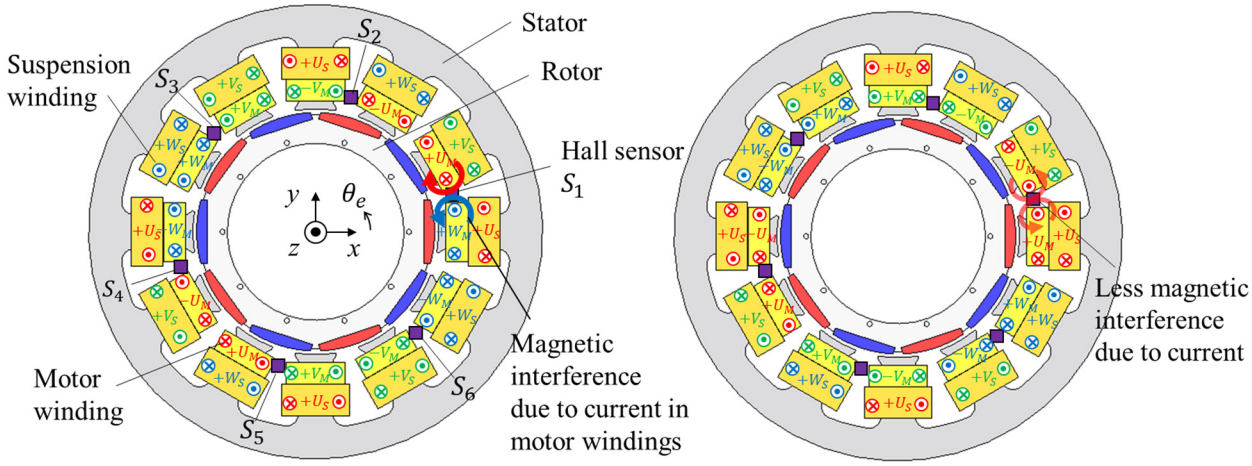

(a) Comparative arrangement (b) Proposed arrangement

Fig. 2 Comparison of the effect of stray flux from motor windings on Hall sensors.

flux will be affected from the left and right motor windings. However, if Hall sensors are placed in a position between the windings of the same phase, as shown in fig. 2(b), the magnetic fluxes have the same magnitude and opposite direction from each other, and theoretically cancel each other out. Also, the winding coefficient of 10 poles 12 slots is higher than that of the 2:3 or 4:3 combinations.

Although not shown in fig. 2, it is also effective to change the positions of Hall sensor, instead of shifting the position of motor windings. It is also assumed to be effective for bearingless motors with integrated windings, which combine motor windings and suspension windings.

3. Open-loop simulation

To analyze the effect of the current of motor windings on six Hall sensors $S_1 \sim S_6$ and the electric angle error $\Delta\theta_e = \hat{\theta}_e - \theta_e$, the finite element method is first compared in an open-loop condition without feedback of the estimated angle $\hat{\theta}_e$ at constant speed 1200 rpm. Figure 3 shows the block diagram. To analyze both DC current and carrier harmonic currents, PWM control with a carrier frequency of 10 kHz is included in the FEM. For the motor in fig. 2, q-axis current

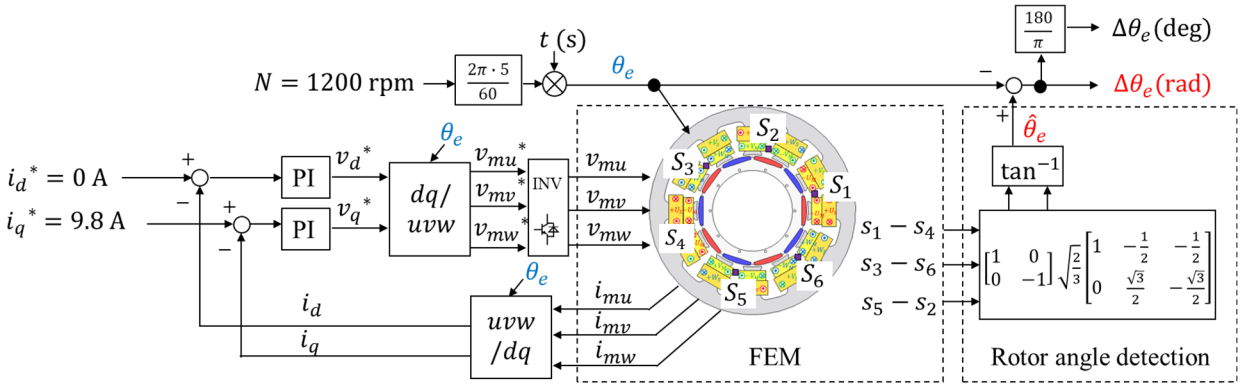

Fig. 3 Block diagram of open-loop simulation. Detected angle $\hat{\theta}_e$ including error $\Delta\theta_e$ is not used in control.

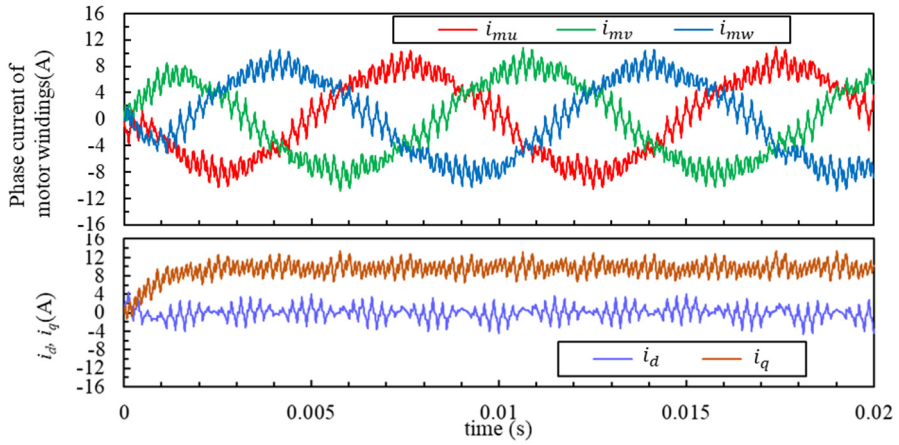

(a) Current waveform in motor windings.

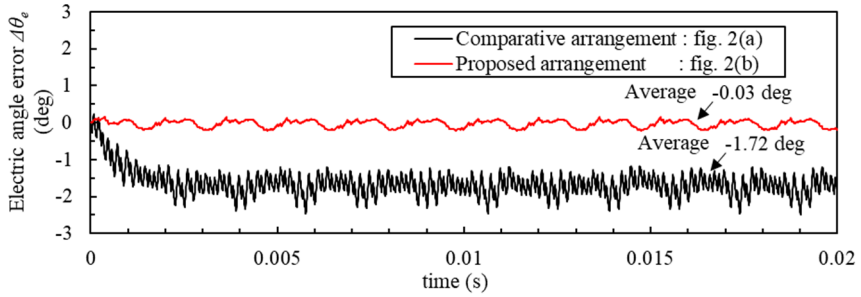

(b) Waveform of electric angle error $\Delta\theta_e$

Fig. 4 Results of open-loop simulation at 1200 rpm, command value $i_q{}^*$ =9.8 A.

i_q changes the phase of the detected flux vector, but d-axis current i_d does not change the phase of detected angle. In other words, d-axis current i_d has a small effect on the angular error, so $i_d = 0$A control is applied.

Figure 4 shows the current waveform and angular error waveform. The q-axis current rises with the start of the simulation, including carrier harmonic components in the waveform. In fig. 4(b), waveform of fig. 2(a) has an angular error in both the DC component and the PWM ripple component due to the q-axis current. The offset error of the detected angle position in the proposed model in fig. 2(b) is reduced, and switching noise is also suppressed. The angle error $\Delta\theta_e$ (rad) can be linearized and expressed as $-k_\theta i_q$, where k_θ (rad/A) is the interference coefficient of current. For model fig. 2(b) versus model fig. 2(a), the coefficient k_θ decreased from $3.0 \cdot 10^{-3}$ to $5.2 \cdot 10^{-5}$. The remaining periodic error in model fig. 2(b) is due to the 5th order spatial harmonics of the permanent magnets.

4. Closed-loop simulation

In Chapter 4, the closed-loop effect of the angle is analyzed in Simulink. Figure 5 shows a definition of coordinate system, and figure 6 shows a block diagram of closed-loop simulation considering $\Delta\theta_e = -k_\theta i_q$. In rotation control, the estimated rotor speed is also distorted by the estimated angle error, which affects speed control. Also, the estimated dq-axis ($\hat{d}\hat{q}$) deviates from the actual dq-axis. The relation of the estimated d- and q-axis currents $i_{\hat{d}}, i_{\hat{q}}$ and the actual d- and q-axis currents i_d, i_q is the expressed in eq. (1).

$$\begin{pmatrix} i_d \\ i_q \end{pmatrix} = \begin{pmatrix} \cos\Delta\theta_e & -\sin\Delta\theta_e \\ \sin\Delta\theta_e & \cos\Delta\theta_e \end{pmatrix} \begin{pmatrix} i_{\hat{d}} \\ i_{\hat{q}} \end{pmatrix} \tag{1}$$

In SPM-type bearingless motors, accurate angle is required for suspension control, and angle error will shift the direction of the suspension force (Chiba et al., 2005, Wellerdieck et al., 2016). In the case of the coordinate system definition and winding arrangement of the model in fig. 2, the relation of the intended x- and y-axis forces $F_{\hat{x}}, F_{\hat{y}}$, and

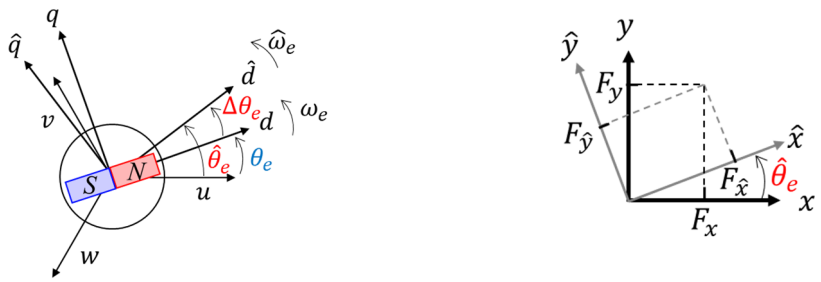

(a) Definition of coordinate system with angle error $\Delta\theta_e$. (b) Suspension force with angle error $\Delta\theta_e$.

Fig. 5 Effect of angle error $\Delta\theta_e$ on motor control and suspension control.

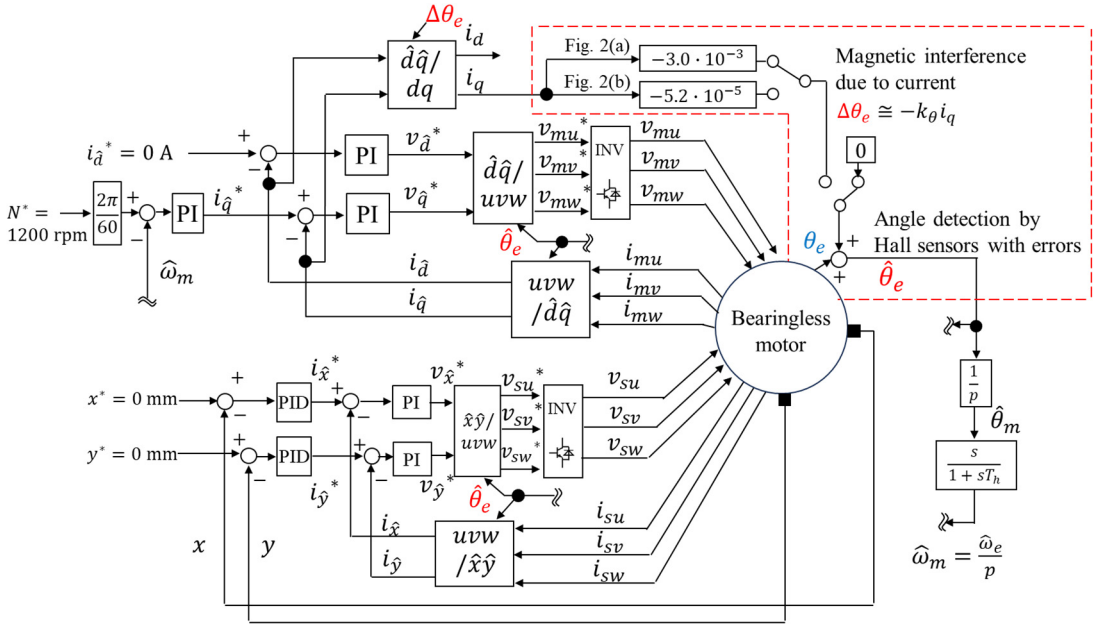

Fig. 6 Block diagram of closed-loop simulation.

the actual x- and y-axis forces F_x, F_y is the expressed in eq. (2).

$$\begin{pmatrix} F_x \\ F_y \end{pmatrix} = \begin{pmatrix} \cos\Delta\theta_e & -\sin\Delta\theta_e \\ \sin\Delta\theta_e & \cos\Delta\theta_e \end{pmatrix} \begin{pmatrix} F_{\hat{x}} \\ F_{\hat{y}} \end{pmatrix} \tag{2}$$

Consequently, angle error $\Delta\theta_e$ may cause vibration of the suspended rotor or increase ineffective currents.

Figure 7 shows a simplified model of the block diagram in fig. 6. The model focuses only on the speed controller, the current controller, and the angle error due to q-axis current i_q. A distinctive feature in fig. 7 is the angle error generated by the current, and its derivative value is added to the real rotor speed ω_m and results in an error in the estimated speed $\hat{\omega}_m$. If the integral gain of the speed controller is assumed to be zero and $\cos\Delta\theta_e$ approximates to 1, the stability condition is expressed by equation 3, where T_c is a coefficient of current controller, T_h is a coefficient of feedback filter, k_P is P-gain of speed controller, k_T is torque coefficient, p is the number of pole pairs, and J is the moment of inertia of the rotor.

$$k_\theta < p\left(\frac{T_c + T_h}{k_P} - \frac{T_c T_h k_T}{J}\right) \tag{3}$$

This means that if the coefficient k_θ is too large, the speed control will diverge.

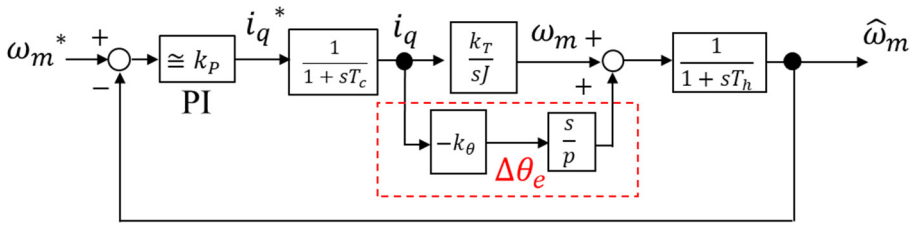

Fig. 7 Simplified model of block diagram in fig. 6.

Figure 8 shows the closed-loop simulation results. In this simulation, suspension force ripple caused by other than detected angle error $\Delta\theta_e$ is ignored, and no compensation for ripple as proposed by Kobayashi et al. (2013) is applied.

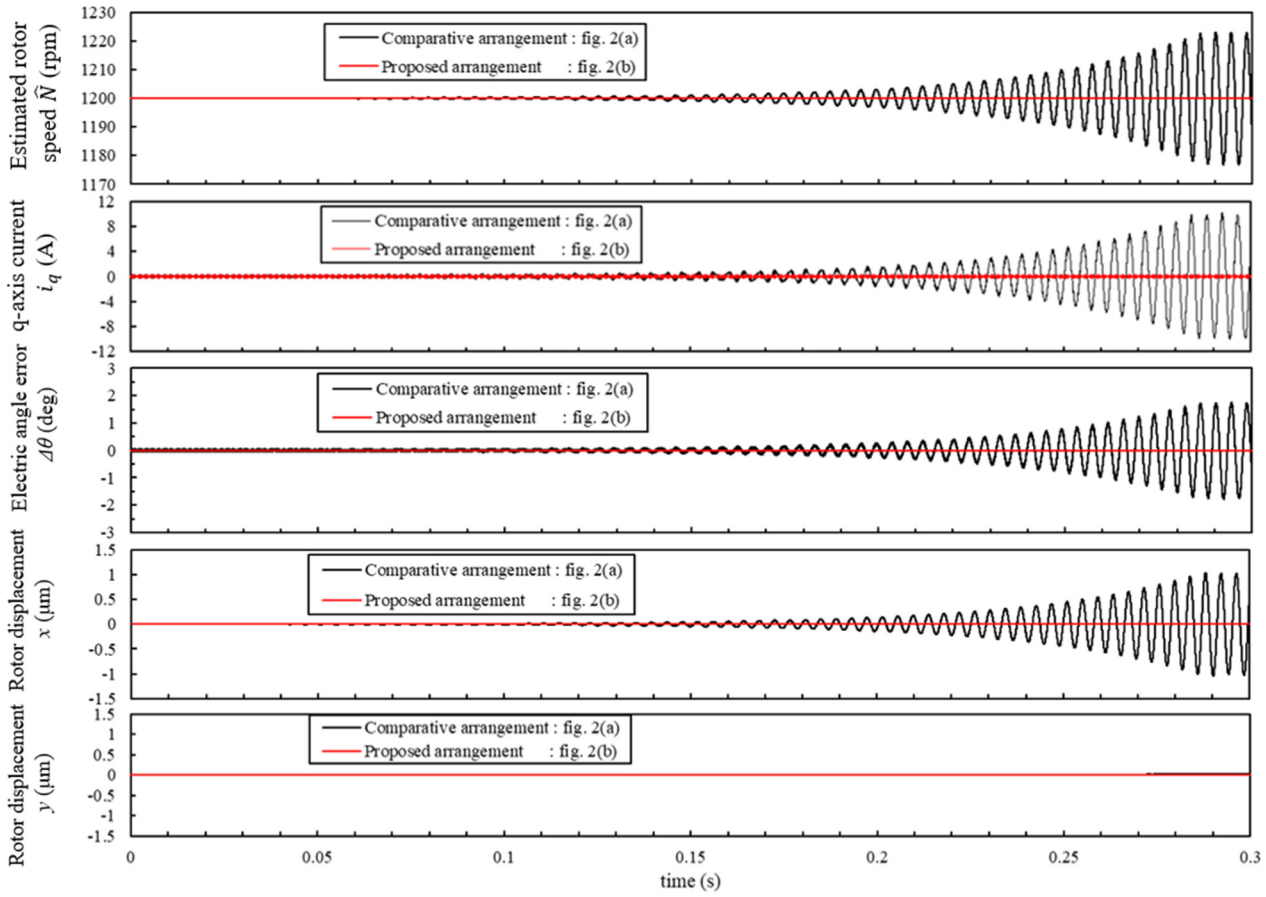

Fig. 8 Result of closed-loop simulation in fig. 6. Superimposition of error $\Delta\theta_e = -k_\theta i_q$ starts at t =0 s. The black line sets k_θ to $3.0 \cdot 10^{-3}$ rad/A, and the red line sets k_θ to $5.2 \cdot 10^{-5}$ rad/A.

A force of 50 N is applied to the rotor in the y-direction as a steady disturbance. From top to bottom, it shows estimated rotor speed $\widehat{N}$ (rpm), q-axis current, angular error $\Delta\theta_e$, x displacement, and y displacement of the rotor. The interference coefficient of current k_θ starts to be reflected in the control at t =0 s. The right side of eq. 3 is calculated to be $3.0 \cdot 10^{-3}$. In the case of $k_\theta = 3.0 \cdot 10^{-3}$ rad/A as the model in fig. 2(a), q-axis current and speed gradually oscillate, and the current value reaches the limiter. Since disturbance force in the y-direction is compensated by the suspension control with angle error, rotor displacement in the x direction is also disturbed. In the case of proposed arrangement in fig. 2(b) as $k_\theta = 5.2 \cdot 10^{-5}$ rad/A, the oscillations of speed, q-axis current and angle error does not occur, and its disturbance on the suspension control is also negligible.

5. Conclusion

This paper shows that angular errors due to motor winding interference can be suppressed by selecting the proposed poles/slots combination and arranging the Hall sensors. The effectiveness is then demonstrated from open-loop and closed-loop control of the detected rotor angle. The proposed method reduces influence of both DC value and PWM harmonics of currents in motor windings. The interference correlation is clarified with block diagrams and mathematical equations, and a stability condition for speed control is presented. By considering the range for stable operation, the divergence of vibration could be avoided in the simulation. This method improves stability and efficiency of bearingless motors without adding components, deteriorating responsiveness, and reducing winding coefficients.

References

P. Peralta, J. Leo and Y. Perriard, "Rotor Position Estimation with Hall-Effect Sensors in Bearingless Drives," 2020 22nd European Conference on Power Electronics and Applications (EPE'20 ECCE Europe), pp. 1-10, 2020.

J. Rao, W. Hijikata, T. Shinshi, “A bearingless motor utilizing a permanent magnet free structure for disposable centrifugal blood pumps”, Journal of Advanced Mechanical Design, Systems, and Manufacturing, Vol. 9, No.3, 2015.

B. S. Weinreb, “A Novel Magnetically Levitated Interior Permanent Magnet Slice Motor,” Master’s thesis, Massachusetts Inst. Technol., Cambridge, MA, USA, 2020.

J. Rudolph, R. Werner and I. Maximow, “Measurement of the Rotor Position of an Active Magnetic Bearing Using Interpolar Stray Flux”, Proceedings of BWMB2013, 2013.

J. Rudolph and R. Werner, “Effect of Eddy Currents on the Stray Flux Based Measurement System for Magnetic Bearing”, Proceedings of ISMB14, pp. 733-736, 2014.

O. Horikawa, R. I. Yamamoto and I. da Silva, “Development of Single Axis Controlled Attraction Type Magnetic Bearing and its Application in Ventricular Assist Device”, Proceedings of BWMB2013, 2013

T. Egawa, T. Mizuno, M. Takasaki, Y. Ishino, and D. Yamaguchi, “Switching Stiffness Control of Lateral Motion in Magnetic Suspension System Using Lateral Displacement Detection with Hall Elements”, Proceedings of ISMB17, pp. 1-10, 2021.

M. Miyoshi, Y. Nakamura, S. Furutani, K. Kajino, and H. Sugimoto, “Proposal of angle detection method for concentrated winding bearingless motors with less magnetic interference due to current”, Electrical Engineering in Japan, Volume 217, Issue 2, e23468, 2024.

A. Chiba, T. Fukao, O. Ichikawa, M. Ooshima, M. Takemoto, and D. Dorell, Magnetic Bearings and Bearingless Drives, 1st ed., Elsevier, 2005.

T. Wellerdieck, P. Reichmuth, D. Steinert, and J. W. Kolar, “Experimental Verification of a Model-Based Zero and Low-Speed Angle Observer for Bearingless Permanent Magnet Machines”, Proceedings of ISMB15, pp. 581-588, 2016.

S. Kobayashi, M. Ooshima and M. N. Uddin, "A Radial Position Control Method of Bearingless Motor Based on d - q - Axis Current Control," in IEEE Transactions on Industry Applications, vol. 49, no. 4, pp. 1827-1835, July-Aug. 2013,